J Solid State Electrochem (2009) 13:733–744
DOI 10.1007/s10008-008-0603-6

ORIGINAL PAPER

Overpotential deposition of copper on gold micro- and nanoelectrodes

Karolina Caban

Received: 10 March 2008 / Accepted: 28 May 2008 / Published online: 25 June 2008

Abstract The mechanism of over-potential deposition of copper on commercial and lab-made gold micro- and nanoelectrodes has been experimentally analysed and compared to the available theoretical descriptions and experimental data. For a larger commercial microelectrode, the measured chronoamperometric transients exhibited a transitional behaviour between the response typical of large Au (111) electrode and the responses recorded for lab-made gold nanoelectrodes. The latter deviated from the theoretical mechanism of Correia, apart from the limiting parts of transients, which showed a partial agreement with the theory. The observed deviations indicate that the role of such parameters as electrode surface area, size, shape and morphology (e.g. defects) is crucial in metal nucleation mechanism at micro- and possibly nano-sized electrodes.

Keywords Electrodeposition · Nucleation · Micro/nanoelectrodes · Copper

Introduction

Electrocrystallization of copper on foreign substrates is a very important technological issue [1–3]. This process is utilized for manufacturing of interconnects, printed-circuit boards, sandwiches of giant magnetoresistive hard disc read heads in electronic industry and in protective and decorative coatings. Apart from the industrial impact, electrodeposition of copper serves as a suitable model system for the fundamental studies on nucleation and growth mechanism. Recently, electrochemical deposition of copper has been utilised for the fabrication of nanoelectrodes and nanowires in a reproducible and controllable manner, which have potential applications in the molecular-scale electronics [4–5]. The aim of this approach is to obtain a nanometer-sized separation that enables electrical contact between the two electrodes *via* tunnelling either directly or after incorporation of an appropriate molecule into a gap.

Narrowing the gap between two electrodes using controlled electrodeposition of copper until achieving the tunnelling distance has been presented in references e.g. [4, 6–8]. These studies are focused mainly on functional aspects of the obtained structures as time changes in the conductance and on their quantized tunnelling properties. Atomic-scale contacts and switches were formed also by reversible repeatable electrodeposition–electrodissolution cycles of silver [9, 10] and platinum [11] onto gold substrate. There are also few literature reports on electrodeposition of gold into a nanogap formed by two gold electrodes [12–15].

In the light of the above facts, the detailed knowledge on the nucleation and growth of copper is needed. Electrodeposition mechanism of copper onto large-surface substrates are now fairly well understood [16–18]. For this reason, despite convenient electrochemistry and "thiol chemistry" of gold, copper is a convenient material to be used for electrochemical preparation of nanocontacts of atomically controlled separation. Thus, although there is only little data about the mechanism of Cu deposition at a nanoscale (e.g. in a gap separating two metal electrodes facing each other), this process often serves as a helpful tutorial for nanoscale deposition of other metals.

Overpotential deposition (opd) of copper, which is also known as bulk deposition, consists of nucleation and growth of two- and three-dimensional metal clusters, which finally form a thicker metal overlayer. The growth of nuclei is determined by the rate of incorporation of new metal atoms, usually by their

K. Caban (✉)
Research Centre Jülich,
Institute for Bio- and Nanosystems IBN-2,
Leo-Brandt Strasse,
52 428 Jülich, Germany
e-mail: k.caban@fz-juelich.de

diffusion. At each nucleus, a localised spherical diffusion field is developed. Individual diffusion fields overlap as the growth of nuclei advances and their coalescence is reflected in characteristic maxima in the initial parts of chronoamperometric transients. These phenomena have been extensively discussed in several papers [16–20] and described qualitatively and quantitatively. The corresponding mathematical treatment has been proposed already more than 20 years ago, first in a very simplified manner by Abyaneh and Fleischmann [21] and later by Abyaneh [22], who applied more elaborated approach. Later, Scharifker and Hills [18] formulated "reduced-variable" plots as a criterion for distinguishing between instantaneous and progressive nucleation. The above mathematical route predicts a conventional diffusion-controlled Cottrellian behaviour of the current after sufficiently long electrocrystallisation time and the occurrence of a maximum in chronoamperometric transients, which is attributed to the overlap of spherical diffusion zones. The model of Scharifker and Hills is, however, applicable only to macroscopic electrodes. An analytical expression for the current at a microelectrode, assuming diffusion control conditions and hemispherical growth, has not been known for many years. Rather recently, Correia et al. [23, 24] have proposed a solution based on the combination of the approach of Scharifker and Hills with that of Aoki and Osteryoung [25] for chronoamperometric transients at disc ultramicroelectrodes. They arrived at separate analytical expressions for chronoamperometric transients related to instantaneous and progressive nucleation.

In this work, the mechanism of overpotential deposition of Cu on microelectrode and nanoelectrodes was analysed applying the approach of Correia, and compared to that observed on large Au (111) surface. We have observed a good agreement between the experimental data for Cu opd on Au(111) and the postulated progressive nucleation mechanism. The application of Correia's method to our experimental data for Cu nucleation at micro- and nanoelectrodes did not produce a satisfactory agreement, which was postulated in references [23, 24] for Cu and Hg deposition on Pt microelectrodes. However, nanoelectrodes used by us were much smaller than microelectrodes applied by Correia. This indicates some limitations of his theory when very small surfaces are considered and suggests that the mathematical description of chronoamperometric opd transients corresponding to nucleation—and—growth at nanoelectrodes still requires much improvement.

Experimental

Electrochemical measurements were performed in a three-electrode cell using a home-made low-noise potentiostat. Pt wire was utilised as a counter electrode. All solutions were purged with Ar for 15–20 min before the measurement was started.

For electrodeposition of Cu, three sizes of gold electrodes were used: large Au(111) bead electrode, surface area 0.0408 cm^2; Au polycrystalline microelectrode (BAS, 5 μm in radius) and polycrystalline Au nanoelectrodes of different surface areas. Au nanoelectrodes were prepared in our lab.

Cleaning of electrodes

Between the measurements, Au(111) single crystal was stored in concentrated H_2SO_4 solution and rinsed thoroughly with water before use. Then, it was flame-annealed in a butane flame for 10 min and cooled down in a stream of argon.

Au microelectrode was polished on a cleaning pad wetted with Al_2O_3 suspension. Oxide particles remaining on the surface were subsequently removed using an ultrasonic bath and a direct stream of water.

Gold nanoelectrodes were rinsed carefully with water in order not to damage the polyethylene coating. During the measurements, they were mounted in the cell using a special Teflon holder. Scanning electron microscopy (SEM) image of exemplary nanoelectrode is shown in Scheme 1.

Fabrication of nanoelectrodes

Fabrication of gold nanoelectrodes proceeded in two main steps: electrochemical etching and coating with polyethylene.

In order to etch 0.5 mm-in-diameter gold wire, it was immersed at a depth of 1 mm into the 1:1 solution of ethanol and concentrated HCl. Then, AC voltage of 25–28 V amplitude and approximately 50 kHz frequency was applied to the wire. When the current started to drop rapidly, the frequency was decreased maximally. The etching procedure was continued until the current was approximately 0.005 A. The shape of the obtained gold nanoelectrode was inspected using the optical microscope.

The etched wire was coated with polyethylene. The coating procedure is shown in Scheme 2. In the holder of the micrometric screw, a gold nanoelectrode was fixed from its blunt end. To the soldering gun, the metal plate with a small hole was fixed. Using the micrometric screw, the nanoelectrode was drawn up so that it protruded through the hole of the metal plate. Then, small pieces of polyethylene were placed on the plate close to the nanoelectrode, and they were heated using the soldering gun. When the polymer became liquid, then the position of the nanoelectrode was lowered so that its apex was immersed into the polymer. Subsequently, the heating was switched off, and the nanoelectrode was moved up and down for several times until polyethylene became sufficiently dense. Then, the nano-

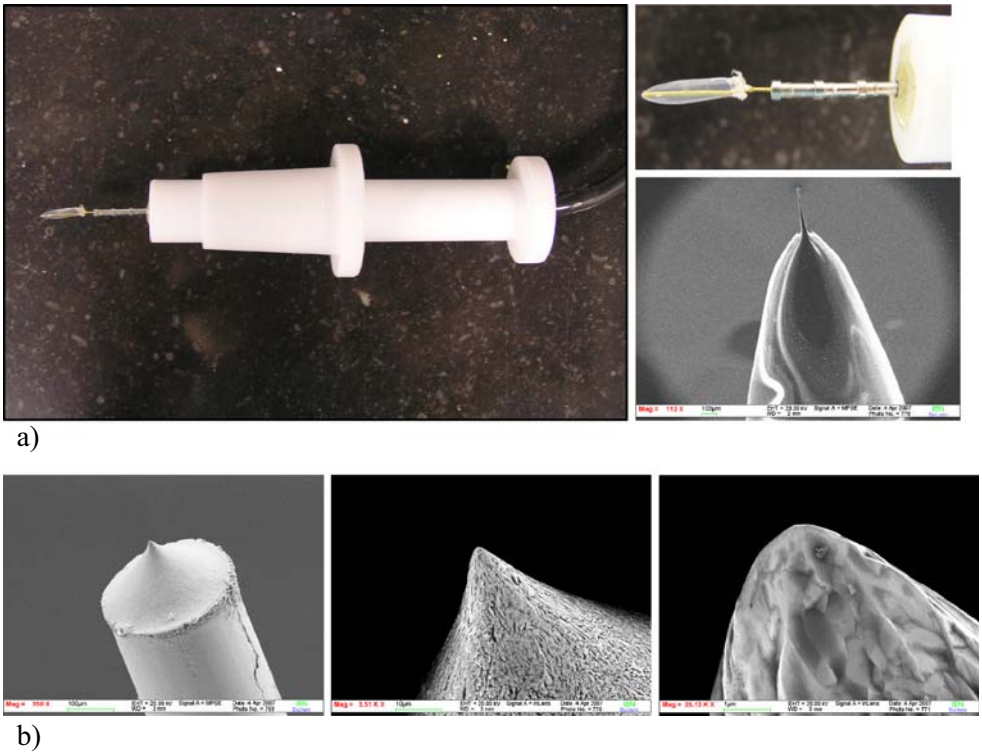

Scheme 1 a Gold lab-made microelectrode mounted in Teflon holder; SEM image of the coated electrode (magnification ×112). **b** Sequential magnification of the very apex of uncoated gold tip; magnification (from *left to right*): ×350, ×3.51 K, ×35.13K

electrode was moved up for the last time and left in this position for a short time to allow the polymer to solidify. During the last upward movement of the nanoelectrode, its sharp apex pierces the coating so that it remains uncovered and provides electric contact with the solution. The smallest uncovered areas were the most required.

Test of electrodes performance

Before copper deposition, voltammetric performance of all gold electrodes was checked in 0.1 M H_2SO_4 solution vs. trapped hydrogen reference electrode, which is a conventional procedure [26, 27]. Active surface areas of gold

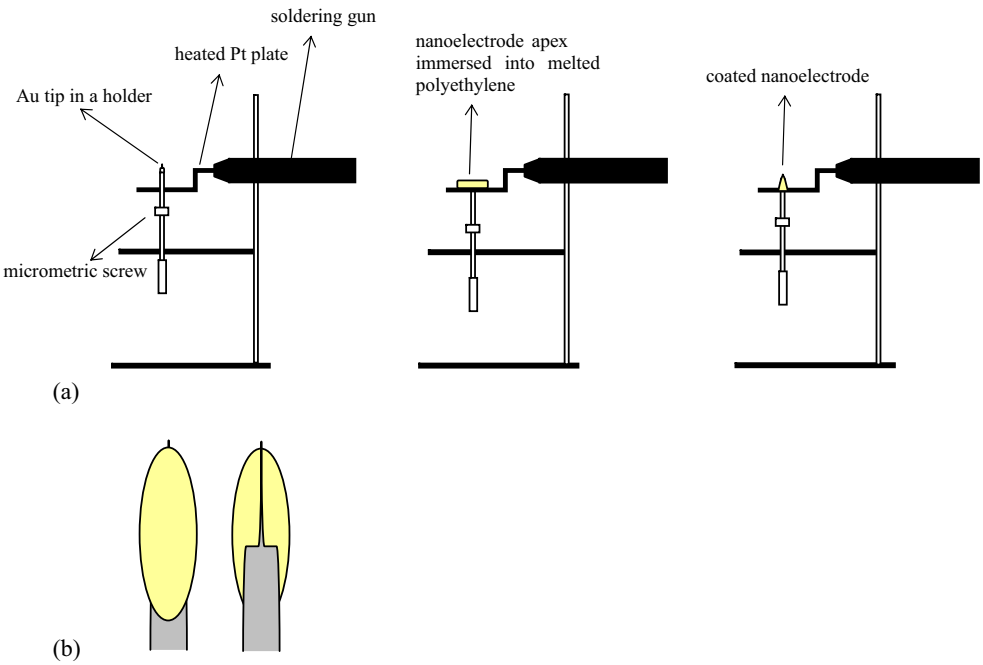

Scheme 2 a The procedure of coating with polyethylene; **b** coated Au nanoelectrode

electrodes were estimated from the charge corresponding to the reduction peak of surface gold oxide and from voltammetric current responses recorded in 1 mM $K_4Fe(CN)_6$ + 0.1 M Na_2SO_4 solution vs. $Hg/HgSO_4$ reference electrode.

Cu electrodeposition was performed from the following solution: 0.1 M Na_2SO_4 + 1 mM H_2SO_4 + 1 mM Cu^{2+} (dissolved CuO). The Cu/Cu^{2+} system was employed as the reference electrode.

The reagents used were purchased from Sigma-Aldrich and Merck.

Water was purified using a Milli-Q system (Millipore).

Results and discussion

Electrochemical performance of gold electrodes and estimation of their surface areas

Voltammetric performance of all gold electrodes was tested in 0.1 M H_2SO_4 and 1 mM $K_4Fe(CN)_6$ solutions.

Exemplary test voltammograms obtained in 0.1 M H_2SO_4 solution are shown in Fig. 1. The response of Au (111) electrode exhibits a typical peak at approximately +0.65 V corresponding to the lifting of surface reconstruction, and a pair of sharp spikes at approximately +1.1 V corresponding to the ordering within the adsorbed hydrogen sulphate adlayer [28].

Anodic peak in the voltammogram recorded for gold microelectrode exemplifies electrochemically induced formation of surface gold oxide; this anodic peak is followed by the sharp spike in the reverse cathodic scan corresponding to the oxide stripping. This is a typical electrochemical behaviour of polycrystalline gold in sulphuric acid medium [29]. Similar voltammetric response was observed for gold nanoelectrode.

Cyclic voltammograms of micro- and nanoelectrodes obtained in H_2SO_4 were used to approximately estimate the surface areas of the investigated electrodes. The calculations were based on the charge corresponding to the reduction peak of the surface oxide. The charge-to-area ratio was assumed 400 $\mu C/cm^2$, as it is usually considered for regular polycrystalline gold electrodes [30].

Exemplary voltammetric responses of selected gold electrodes measured in 1 mM $K_4Fe(CN)_6$ solution are presented in Fig. 2. $K_4Fe(CN)_6$ is a model redox compound in electrochemistry of the well-known diffusion coefficient (0.735×10^{-5} cm^2/s [31]), which gives stable, reproducible and reversible cyclic voltammetric (CV) responses. The differences between the voltammograms shown in Fig. 2 do not arise from the crystalline structure of the gold electrodes used but are related to their sizes. Mass transport of the $K_4Fe(CN)_6$ redox probe in case of relatively large Au(111) electrode is controlled by linear diffusion, while in case of gold micro/nanoelectrodes by spherical diffusion. Consequently, at a large electrode, the thickness of the diffusion layer increases in time and develops towards the bulk leading to the progressive depletion of the redox probe in the vicinity of the gold surface. The measured diffusion-controlled voltammetric current, after reaching maximum, progressively decreases. In contrast, the thickness of spherically shaped diffusive layer at the micro/nanoelectrode surface remains almost constant during the CV potential scan providing constant in time Faradaic current [32]. Thus, respectively for both cases, peak- and wave-shaped voltammograms were obtained. In the linear diffusion regime, there is a linear relationship between the magnitude of the voltammetric peak and the electrode surface. In the spherical diffusion regime, the magnitude of the steady-state current is proportional to the microelectrode radius. These proportionalities are quantified by Eqs. 1

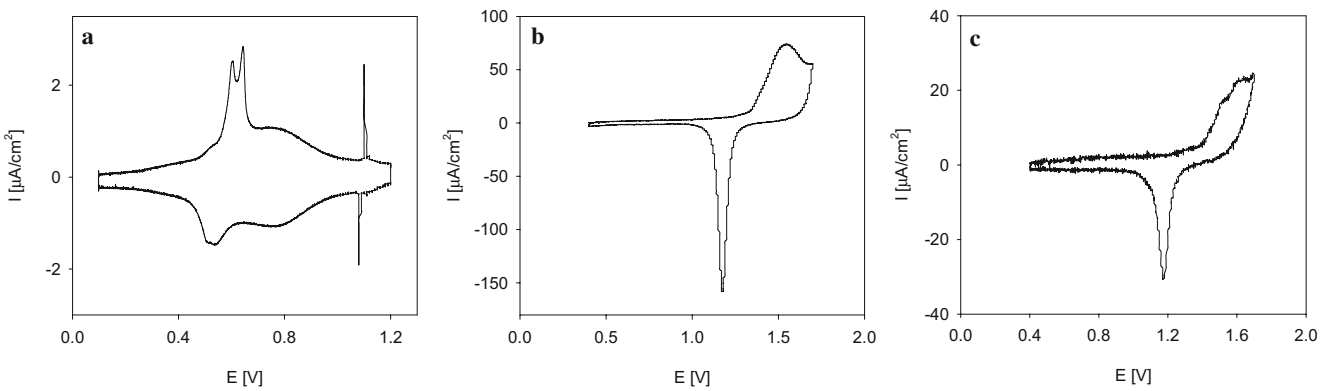

Fig. 1 Cyclic voltammograms of Au (111) electrode (**a**), Au microelectrode (**b**) and Au tip nr 2 (**c**) obtained in 0.1 M H_2SO_4 solution; scan rate, 10 mV/s; reference electrode, H_2/H^+

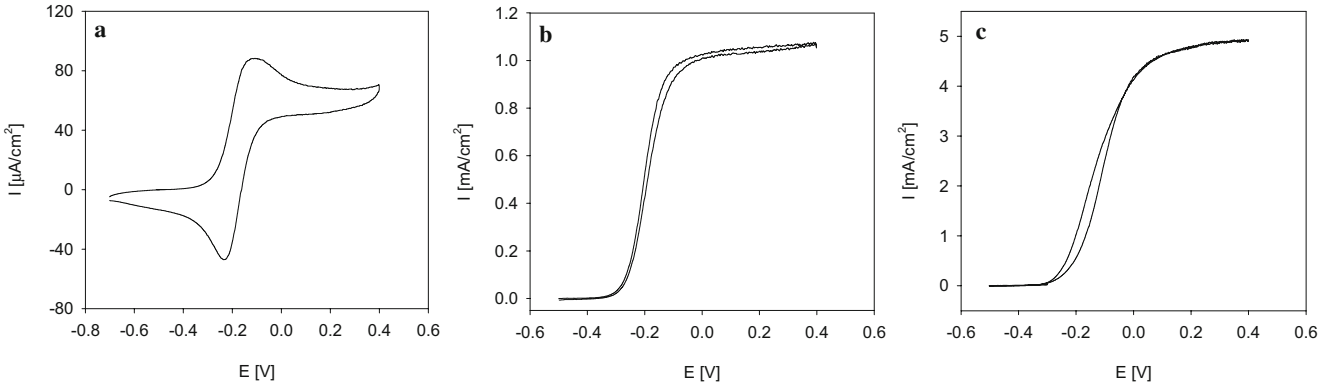

Fig. 2 Cyclic voltammograms of Au (111) electrode (**a**), Au microelectrode (**b**) and Au tip nr 2 (**c**) obtained in 1 mM $K_4Fe(CN)_6$ solution; supporting electrolyte: 0.1 M Na_2SO_4; scan rate, 10 mV/s; reference electrode, sat. $Hg/HgSO_4$ (potential shift vs. H_2/H^+: +0.658 V)

and 2 shown below. Randles–Sevčik equation (Eq. 1) was employed to calculate the surface area of Au(111):

$$I_{peak} = 0.4463nFAC\left(\frac{nvFD}{RT}\right)^{1/2} \quad (1)$$

where n is the number of electrons per ion/molecule oxidised or reduced (here, n=1), F the Faraday constant, A the Au (111) electrode surface area, C bulk concentration of electroreactant (here, 1 mM), v the scan rate (here, 10 mV/s), D the bulk diffusion coefficient of $K_4Fe(CN)_6$ (0.735×10^{-5} cm^2/s) and R the gas constant. Similarly, the expression for the steady-state limiting voltammetric current,

$$I_{ss} = 4nFDCr \quad (2)$$

where n is the number of electrons per ion/molecule oxidised or reduced, F the Faraday constant, D the bulk diffusion coefficient of $K_4Fe(CN)_6$, C the bulk concentration of electroreactant and r electrode radius, was employed to estimate surface areas of micro- and nanoelecterodes. Surface areas of nanoelectrodes were assumed discs.

The calculated surface areas, radii and the corresponding charges and limiting current values are summarised in Table 1. Noteworthy, the numbers obtained for nanoelectrodes have only rough meaning as their very apexes are in fact most likely the cones (see SEM images in Scheme 1). The surface areas of nanoelectrodes estimated from CVs recorded in H_2SO_4 and $K_4Fe(CN)_6$ were compared. The results were rather consistent; however, for some nanoelectrodes, some deviations were observed. Thus, it was difficult to judge if the agreement between the surface areas estimated for particular nanoelectrodes in both solutions can be considered as a criterion of a good performance of these electrodes. For example, the voltammograms of nanoelectrode no. 2 obtained in H_2SO_4 and $K_4Fe(CN)_6$ exhibited almost perfect shapes, and the surface areas estimated from both measurements agreed quite well. For some other nanoelectrodes, voltammetric responses exhibited correct shapes, but the calculated surface areas were inconsistent. Due to the above difficulties, for copper deposition one used five nanoelectrodes (no. 2, 3, 4, 16 and 19 in Table 1) with respect to either their small dimensions or the most regular voltammetric responses in 0.1 M H_2SO_4 and 1 mM $K_4Fe(CN)_6$ solutions. The surface areas obtained in both measurements were averaged before they were used as normalising factors for the calculation of current densities.

For the microelectrode, there was an inconsistence between the surface area estimated from cyclic voltammograms recorded in 0.1 M H_2SO_4 and 1 mM $K_4Fe(CN)_6$. However, after averaging, the obtained value was very close to the geometric surface area. For this reason, in further calculations, geometric radius of 5 μm was used.

Also in case of a large Au(111) bead electrode, the geometric radius was used in the calculations.

Under- and over-potential deposition of copper on gold electrodes

Under- and overpotential (bulk) electrodeposition of copper was performed at a large-sized Au(111) bead electrode and polycrystalline micro- and nanoelectrodes. Voltammetric upd and chronoamperometric opd responses obtained at nanoelectrodes and at a microelectrode were compared to that of gold single crystal, which served as the reference.

Under- and over-potential deposition of copper on Au(111) bead electrode

The voltammogram corresponding to Cu upd deposition on Au(111) was recorded by scanning the potential from the positive to the negative direction, and backwards, Fig. 3a. It exhibits a shape typical for the three-step formation of a copper monolayer [17]. In the potential range 0.6–0.35 V

Table 1 Geometric and estimated radii and active surface areas of the used gold electrodes

	Geometric radius and surface		Estimated radius and surface					
			CV in H_2SO_4			CV in $Fe(CN)_6^{4-}$		
	Radius (μm)	Surface (cm^2)	Charge × 10^{-11} (Q)	Radius (μm)	Surface × 10^{-7} (cm^2)	I_{ss} or I_{peak} (nA)	Radius (μm)	Surface × 10^{-7} (cm^2)
Au(111)	11.4×10^2	0.0408				3.59×10^3	12.48	0.0489
Commercial Au microelectrode	5	7.85×10^{-7}	87.7	7.90	19.6	0.827	2.91	2.66
lab-made Au microelectrode								
No. 2			3.93	1.77	0.98	0.68	2.40	1.81
3			6.79	2.32	1.70	0.63	2.22	1.52
4			1.58	1.12	0.40	0.31	1.09	0.38
5			5.19	2.03	1.30	0.67	2.36	1.81
8			4.53	1.90	1.13	0.55	1.94	1.18
13			12.1	3.10	3.02	0.98	3.45	3.74
16			15.1	3.46	3.76	0.415	1.46	0.67
18			9.36	2.73	2.34	0.23	0.81	0.21
19			6.64	2.30	1.66	2.0	7.05	15.6
21			2.65	1.45	0.66	0.30	1.06	0.35

The values were estimated from the test experiment in 0.1 M H_2SO_4 and 1 mM $K_4Fe(CN)_6$ solutions. Surfaces of lab-made microelectrodes were assumed discs.

Cu atoms are adsorbed randomly at a low coverage. A pair of peaks at approximately +0.2 V corresponds to the formation of a honeycomb structure of Cu atoms that covers two thirds of the whole available surface. In this structure, Cu atoms form hexagons, in which sulphate ions are trapped and co-adsorbed. In the third step, a complete Cu layer is deposited in the potential window of approximately 0.08–0.02 V and Cu atoms reside in threefold hollow sites of Au(111).

Bulk deposition of copper was induced by extending the potential window shown in Fig 3a to a more negative direction. Potential values corresponding to overpotential deposition of Cu were in the range −0.15–−0.2 V. Potentials from this range were subsequently selected for chronoamperometric investigations of the mechanism of Cu opd and its dependence on the electrode surface area.

Exemplary series of chronoamperometric responses are shown in Fig. 4a. Each response corresponds to the potential jump from +100 mV to the value from the opd range −50–−150 mV. Conditioning step at +100 mV lasted 10 s and was applied in order to deposit some metal under upd conditions and therefore to remove the corresponding upd current from the subsequent opd chronoamperometric signal. Prolonged bulk deposition of copper was avoided in order to prevent alloying between copper and Au substrate. Between the consecutive runs, the electrode was kept for 2–3 min at +600 mV in order to dissolve Cu deposited on the surface in the former scan.

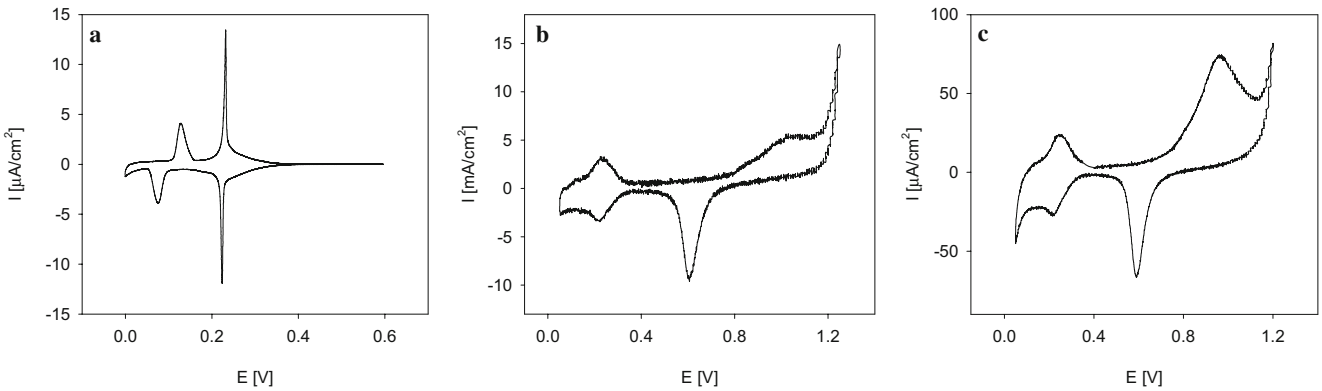

Fig. 3 Cyclic voltammograms of copper upd obtained at: Au (111) (**a**), Au microelectrode (**b**) and Au tip nr 2 (**c**); solution: 1 mM Cu^{2+} (dissolved CuO) + 0.1 M Na_2SO_4 + 1 mM H_2SO_4; scan rate, 1 mV/s (**a**) and 10 mV/s (**b**, **c**); reference electrode: sat. Cu/Cu^{2+} (potential shift vs. H_2/H^+: +0.316 V)

In almost all chronoamperograms shown in Fig. 4a, a maximum in the initial part of each transient is visible. The magnitude of this maximum depended on the conditioning potential (preceding the jump to the opd region) and increased when this potential was increased from +100 to +150 mV. Duration of the conditioning potential step (5, 10, 20 and 30 s) at +150 mV had no influence on the recorded chronoamperometric behaviour.

Chronoamperograms for Au(111) shown in Fig. 4a are consistent with the literature data and also agree well with the transients for Au polycrystalline electrode [33]. In the very initial part of transients, one observes rapidly decreasing charging current. Subsequently, the current starts to increase fast due to nucleaction and growth of copper nuclei. These nuclei progressively merge in time, and their spherical diffusion zones overlap to form a single thick diffusion zone. This corresponds to the current maximum; after reaching maximum, the current decays according to the diffusion-controlled mechanism and chronoamperometric transient tends to approach the plot expected for diffusion control. The position of the current maximum at Au (111) electrode and on polycrystalline gold electrode shifts to shorter times with the increasing negative opd potential.

Theoretical Cottrellian plot (dashed line) calculated for Au(111) disc electrode of 0.0408 cm^2 in area according to equation:

$$I(t) = \frac{nFADC}{\sqrt{\pi Dt}} \tag{3}$$

where D is a diffusion coefficient of Cu^{2+} (0.714×10^{-5} cm^2/s), C denotes bulk concentration of Cu^{2+} (1 mM), and other symbols have usual meanings, coalesces with the experimental transients after approximately 9–10 s of Cu deposition. At shorter deposition times but already after the maximum, the experimental current densities are lower than the theoretical Cottrellian value. Possibly, at the initial stage of metal deposition, several individual nuclei are formed, each accompanied by separate spherical diffusion zone. One may anticipate that the total active surface area of the formed nuclei is smaller than the initial surface area of Au(111) electrode assumed in all calculations. Consequently, the calculated densities of the experimental transients are underestimated. This might explain why experimental current densities are lower than the current density corresponding to the theoretical Cottrellian plot. However, true surface areas at each stages of copper deposition are not known and can not be incorporated into the calculations.

After some time, when deposition of copper advances, individual nuclei merge; consequently, the final surface area becomes flat again and does not differ significantly from the initial area. In other words, there is a contribution from spherical diffusion to individual copper nuclei only at relatively short deposition times. Afterwards, a transition from spherical to linear diffusion takes place. This is facilitated by more negative potentials, which favour faster nucleation-and-growth process. Accordingly, the measured chronoamperometric transients approach the theoretical plot after shorter times.

The obtained series of chronoamperometric transients allowed one to judge on the nucleation mechanism. In general, one distinguishes two types of nucleation mechanism: instantaneous and progressive. This division is based on the nucleation rate. At high nucleation rates (instantaneous nucleation), all nuclei are formed immediately after imposition of the potential; they grow at the same rate so that they are all of the same age and their number remains constant. At low nucleation rates, the number of nuclei is progressively increasing (progressive nucleation), and they exhibit different stadia of growth.

A simple criterion that allows one to distinguish between these two mechanisms at a macroscopic electrode is a comparison of "reduced-variable" plots: $(I/I_{max})^2$ vs. (t/t_{max}), where I_{max} and t_{max} denote the maximum current value and the corresponding time. Theoretical plots are described by the following formulas:

$$(I/I_{max})^2 = \frac{1.9542}{(t/t_{max})}\{1-\exp[-1.2564(t/t_{max})]\}^2 \tag{4}$$

and

$$(I/I_{max})^2 = \frac{1.2254}{(t/t_{max})}\left\{1-\exp\left[-2.3367(t/t_{max})^2\right]\right\}^2 \tag{5}$$

for instantaneous and progressive nucleation, respectively [18]. Experimental "reduced-variable" plots corresponding to Cu opd at Au(111) surface are presented in Fig. 5. Theoretical curves are included as dashed lines. There is an excellent agreement between the theoretical plot predicted for progressive nucleation and the experimental plots.

Under- and over-potential deposition of copper on gold micro- and nanoelectrodes

Voltammetric responses of gold microelectrode and a selected nanoelectrode (no. 2) corresponding to underpotential deposition of copper are shown in Fig. 3b and c. A peak at approximately +0.6 V corresponds to reduction of AuO_x. A pair of peaks at approximately +0.1–+0.15 V refers to the upd formation of a complete copper overlayer. Some aspects of underpotential deposition of Cu on polycrystalline electrodes have been described in references [34, 35].

Bulk deposition of copper was performed by scanning the potential up to −0.15–−0.2 V. Non-steady state features in chronoamperometric responses at micro- and nanoelectrodes were analysed in order to get a deeper insight into

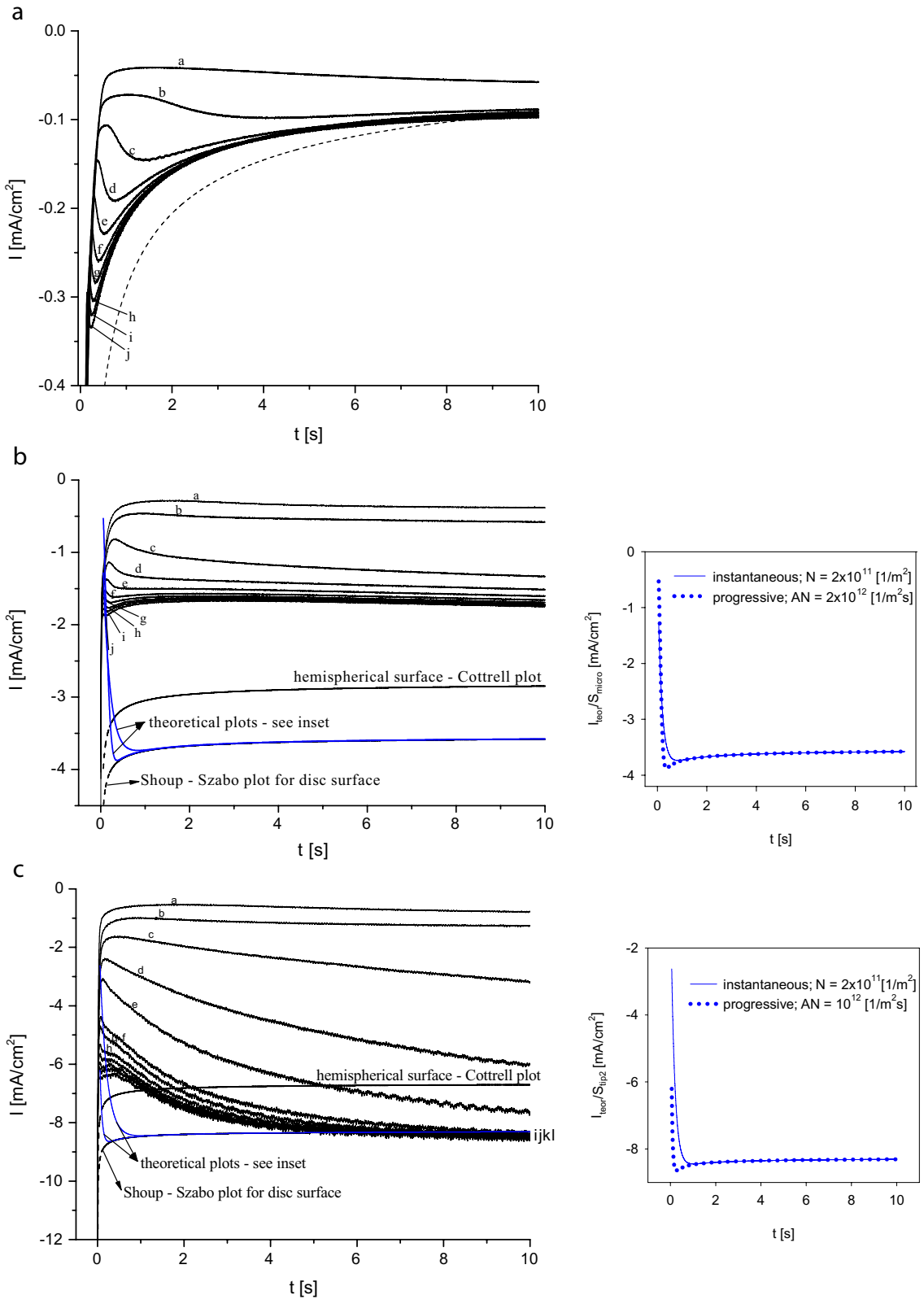
a
I [mA/cm²]
t [s]
b
I [mA/cm²]
t [s]
hemispherical surface - Cottrell plot
theoretical plots - see inset
Shoup - Szabo plot for disc surface
I_teor/S_micro [mA/cm²]
instantaneous; N = 2x10¹¹ [1/m²]
progressive; AN = 2x10¹² [1/m²s]
t [s]
c
I [mA/cm²]
t [s]
hemispherical surface - Cottrell plot
ijkl
theoretical plots - see inset
Shoup - Szabo plot for disc surface
I_teor/S_tip2 [mA/cm²]
instantaneous; N = 2x10¹¹[1/m²]
progressive; AN = 10¹² [1/m²s]
t [s]

◀ **Fig. 4** **a**. Chronoamperometric responses of Au (111) electrode in the solution of 1 mM Cu^{2+} (dissolved CuO) + 0.1 M Na_2SO_4 +1 mM H_2SO_4 (supporting electrolytes). Each response corresponds to the potential step from + 100 mV (duration time, 10 s) to −60÷-150 mV, each 10 mV (duration time, 20 s; curves *a* → *j*). Between consecutive runs electrode was kept at +600 mV. Reference electrode, Cu/Cu^{2+}. Currents are normalised with respect to the electrode area (0.0408 cm^2). *Dashed line* Theoretical Cottrellian transient. **b** Chronoamperometric responses of Au microelectrode in the solution of 1 mM Cu^{2+} (dissolved CuO) + 0.1 M Na_2SO_4 +1 mM H_2SO_4 (supporting electrolytes). Each response corresponds to the potential step from + 150 mV (duration time: 10 s) to -70÷-160 mV, each 10 mV (duration time: 20 s; curves a → j). Between consecutive runs electrode was kept at + 600 mV. Reference electrode, Cu/Cu^{2+}. Currents are normalised with respect to the disc electrode surface area (7.85×10^{-7} cm^2). *Dashed line* Theoretical Cottrellian transient for hemispherical microelectrode; *dotted line*, theoretical Shoup–Szabo transient for disc microelectrode; *blue lines*, theoretical transients for progressive and instantaneous nucleation at microelectrode (magnification on the right side; for details see text). **c** Chronoamperometric responses of Au tip (no. 2) in the solution of 1 mM Cu^{2+} (dissolved CuO) + 0.1 M Na_2SO_4 +1 mM H_2SO_4 (supporting electrolytes). Each response corresponds to the potential step from + 150 mV (duration time, 10 s) to −50–−180 mV, each 10 mV except from −60 and −110 mV(duration time, 20 s; curves *a* → *l*). Between consecutive runs electrode was kept at +600 mV. Reference electrode, Cu/Cu^{2+}. Current is normalised with respect to the electrode surface area (1.395×10^{-7} cm^2). *Dashed line* Theoretical Cottrellian transient; *blue lines* theoretical transients for progressive and instantaneous nucleation at microelectrode (magnification on the right side; for details see text)

the copper nucleation mechanism. The applied potential programme was the same as that described in "Under- and over-potential deposition of copper on Au(111) bead electrode for Au(111)"; instead of 100 mV, one applied 150 mV as the conditioning potential. Chronoamperometric transients shown in Fig. 4b and c correspond to the potential step from +150 mV to the selected values from the opd range. Conditioning step at +150 mV initialised underpotential deposition of copper and allowed one to remove the corresponding upd current from the subsequent opd chronoamperometric signal.

Some chronoamperograms in Fig. 4 exhibit a maximum in the initial part of each transient. However, compared to chronoamperometric opd transients for Cu at the macroscopic Au(111) electrode, these obtained at gold microelectrode exhibit much less pronounced maximum, while for nanoelectrode the maximum disappears almost completely. Very similar differences between the chronoamperometric transients obtained for micro/nanoelectrodes and the response of Au disc polycrystalline electrode of the similar surface area (0.038 cm^2) [33] to that of Au(111) electrode used in this study (0.0408 cm^2) were observed. As it was already mentioned before, the shapes of chronoaperometric transients for Au polycrystalline and Au (111) electrodes are very consistent.

The above facts clearly show that there is a relation between the magnitude of the maximum and the electrode surface area, and indicate different nucleation process for variously sized electrodes; the influence of the surface structure of gold (polycrystalline vs. single-crystal) is of much less importance in the light of the performed studies.

The same chronoamperometric behavior as for nanoelectrode no. 2 was observed also for other investigated nanoelectrodes, with small deviations. These deviations might be attributed to the following factors: nucleation mechanism possibly depends not only on the electrode area but also on its shape; upd chronoamperometric signal partially contributes to the measured opd response and real surface areas of nanoelectrodes are different from the roughly estimated values given in Table 1.

The results obtained for the microelectrode is consistent with that obtained by Hills et al. [36] for potentiostatic deposition of mercury on 4-μm in-radius carbon fibre electrode and by Correia et al. [23, 24] for potentiostatic deposition of copper and mercury on Pt microelectrode of 20 μm in radius.

In case of nanoelectrodes and, to some extent, also in case of microelectrode, it was expected that the number of nuclei generated at the surface is rather limited and most probably only few, or even a single one, are formed. According to Hills et al. [36], only one nucleus is formed each 30 s onto the surface area of 10^{-10} m^2 assuming the highest nucleation rate. This process may be even slower in

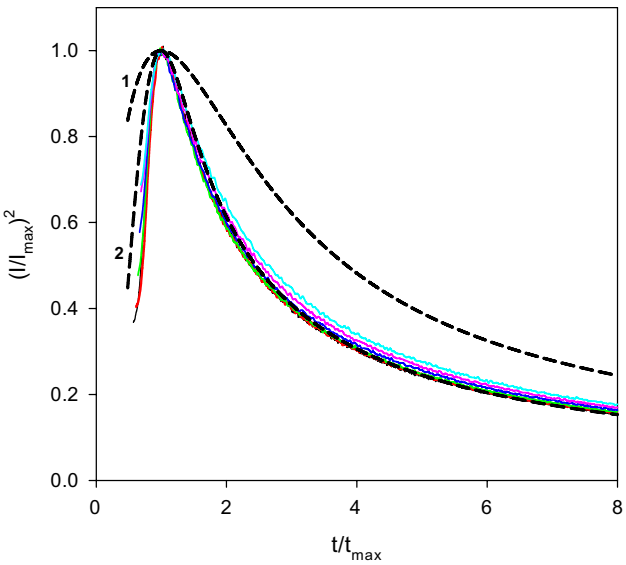

Fig. 5 Chronoamperometric current transients (reduced-variable plots) for Cu opd on Au (111); solution, 1 mM Cu^{2+} (dissolved CuO) + 0.1 M Na_2SO_4 +1 mM H_2SO_4 (supporting electrolytes). *Dotted lines* Calculated curves for instantaneous (*1*) and progressive (*2*) nucleation. *Other lines* Experimental plots corresponding to the potential step from +150 mV (duration time, 10 s) to −90–−140 mV, each 10 mV. Between consecutive runs electrode was kept at +600 mV. Reference electrode, Cu/Cu^{2+}

case of smaller surfaces of nanoelectrodes listed in Table 1. Merging of diffusion fields of only few nuclei should not contribute significantly to the decrease of the surface area, so that the maximum is not formed, or at least, it is pronounced very weakly. Due to somewhat larger surface area of a microelectrode compared to nanoelectrodes, mechanism of nucleation at a microelectrode can be regarded as a transitive between the mechanism observed at large Au(111) surface and on nanoelectrodes.

It was anticipated that after reasonably long time of potentiostatic overpotential deposition of copper at micro- and nano-electrodes the measured currents should approach the limiting values expected for diffusive control of mass transport. Theoretical plots for disc-shaped micro- and nanoelectrodes were constructed employing Shoup and Szabo expression [37]:

$$I(t) = 4nFDCr\begin{pmatrix} 0.7854 \;+\; 0.8862\,\tau^{-1/2} \\ +0.2146\;\exp\left(-0.7823\,\tau^{-1/2}\right) \end{pmatrix}, \qquad \tau = \frac{4Dt}{r^2} \tag{6}$$

where all symbols have their usual meanings and $D = 0.714 \cdot 10^{-5}$ cm^2/s and C=1 mM Cu^{2+}; r is the micro/nanoelectrode radius from Table 1.

Due to the progressive deposition of metal, the surfaces of the gold electrodes might have increased and become spherical. Thus, also a modified Cottrell equation adjusted to spherical diffusion to a microdisc has been used to calculate theoretical current density:

$$I(t) = nFDAC\left(\frac{1}{r} + \frac{1}{\sqrt{\pi Dt}}\right) \tag{7}$$

Both theoretical transients are included in Fig. 4b and c. Consistently with the theory, current density at a disc electrode is higher than at a hemispherical surface. However, experimental currents densities obtained at the microelectrode are much lower than both theoretical values—see Fig. 4b. Possible reasons for this behaviour can be that the amount of deposited copper much exceeds the volume provided for the hemisphere of 5 μm in radius and the corresponding final surface area is much bigger than that assumed as a normalising factor in Fig. 4b. Definitely, due to fast radial diffusion, the increase of the surface area of a microelectrode after metal deposition is much more significant than at a conventionally-sized Au(111) electrode.

Better agreement between the theoretical and experimental chronoamperometric limiting current densities has been found for the nanoelectrode. The experimental values approach the theoretical Shoup–Szabo values after appropriately long deposition time, see Fig. 4c.

Interestingly, in the chronoamperograms recorded at micro- and especially at nanoelectrodes, the transient currents increase to approach the limiting value, while they decrease at the bead Au(111) electrode.

An analytical expression for the opd current assuming diffusion control conditions and hemispherical growth at a microelectrode has not been known for many years. "Reduced-variable" plots (expressions 3 and 4) are true, however only for nucleation mechanism under diffusion control at macroscopic electrodes. Rather recently, Correia et al. [23, 24] combined the model proposed by Scharifker and Hills [18] and expressions derived by Aoki and Osteryoung [25] for chronoamperometric transients at disc ultramicroelectrodes and arrived at separate analytical expressions for chronoamperometric transients at microelectrodes related to instantaneous and progressive nucleation, respectively:

$$I(t) = \left(4nFDCr + 8nFr^2D^{1/2}\pi^{-3/2}t^{-1/2}\right) \cdot \left[1 - \exp(-N\pi kDt)\right] \tag{8}$$

$$I(t) = \left(4nFDCr + 8nFr^2D^{1/2}\pi^{-3/2}t^{-1/2}\right) \cdot \left[1 - \exp\left(-0.5AN\pi k'Dt^2\right)\right] \tag{9}$$

where N is the number of nuclei, AN the rate of nuclei formation, D the diffusion coefficient of copper ion (0.714×10^{-5} cm^2/s), C the molar concentration of metal ions, r the electrode radius, $k = \sqrt{\frac{8\pi CM}{\rho}}$, $k' = \frac{4}{3}\sqrt{\frac{8\pi CM}{\rho}}$, M the molecular mass of deposited copper (63.55 g/mol) and ρ the density of copper (8.93 g/cm^3).

Equations 8 and 9 quantify the I–t transients at disc microelectrodes; they were derived involving diffusion-controlled overlapping and merging of local diffusion zones and radial diffusion.

In order to evaluate chronoamperometric results obtained for micro- and nanoelectrodes, an iterative procedure was used: Several N and AN values were subjected to Eqs. 8 and 9 to obtain the best fit to the experimental plots. Exemplary theoretical plots are included in Fig. 4b and c; for better visualisation, they are also shown in separate insets. They correspond to exemplary $N = 2 \times 10^{11}$ m^{-2} and AN$= 2 \times 10^{12}$ m^{-2} s^{-1} values for instantaneous and progressive nucleation, respectively. For none of the applied N and AN values a good agreement between the theory and the experiment was achieved. Moreover, these values are probably much larger than the number of nuclei really generated on such small electrodes; however, for lower N and AN values, even stronger discrepancies were observed. Nevertheless, theoretical current densities were very consistent, in the limiting current range, with the Shoup–Szabo plots, but they were always higher than the measured values.

Recently, Heerman and Tarallo [38] have modified Correia's approach and proposed more general equations

describing diffusion-controlled nucleation and growth on disc-shaped microelectrodes. Their procedure allows one to extract the nucleation rate constant from chronoamperometric transients and is not restricted only to two limiting cases of progressive and instantaneous nucleation. However, it applies only to the electrodes of diameter ranging between 25 and 100 μm. This is still much too high to be applicable to nanoelectrodes.

Conclusions

Au nanoelectrodes were fabricated by electrochemical etching and consecutively coated with polyethylene to provide the required insulation. Electrochemical performance of the nanoelectrodes was studied, and their active surface areas were estimated. The nanoelectrodes were subsequently used for over- and underpotential deposition of copper. The obtained chronoamperometric transients of Cu opd were compared to these recorded for polycrystalline Au microelectrode and Au (111) bead electrode. Significant differences between the transients followed the decreasing surface areas of the electrodes. The transients at nanoelectrodes exhibited almost no maximum, while those recorded at the microelectrodes showed a transitional behaviour between the responses obtained at large Au (111) and Au nanoelectrodes. The initial parts of transients observed at nanoelectrodes deviated from theoretical plots predicted by Cottrell and Shoup–Szabo equations, as well as from I vs. t dependencies derived recently by Correia for metal deposition on microelectrodes. Partial agreement was found only in the limiting parts of transients.

The differences between the chronoamperometric opd plots recorded for large Au(111) and micro/nanoelectrodes indicate that copper deposition at small-scaled electrodes proceeds differently than at regularly-sized electrodes. However, at this stage, it is difficult to clearly point at the factors responsible for such behavior. Typically, the initial smooth copper monolayer grows two-dimensionally according to the FM (Frank–van der Merwe) mechanism. At a critical thickness, significant strain energy accumulates in the deposited monolayer. This strain induces a switch in the further growth mode to the VW (Volmer–Weber) type. At this point, it is energetically favourable to nucleate islands, since adatom–adatom interactions are stronger than those of adatom to the surface. These phenomena lead to the formation of 3D clusters of islands. This mechanism, covering the transition between the layer-by-layer approach (FW) to islands-based growth at the critical layer thickness (VW) is known as Stranski–Krastanov [39] intermediary mechanism that combines 2D layer and 3D island growth and results from the interplay between surface and interface energies and strain energy. The growth of nuclei is determined by the rate of incorporation of new metal atoms, usually by their diffusion.

It is difficult to judge based on the presented experimental results if the mechanism of Cu opd differs much between macro-, micro- and nanoelectrodes. However, some modifications of the SK mechanism with respect to the area-limited number of nuclei and their formation rate on variously sized and shaped electrodes should be considered. As mentioned before, decreasing the value of N in Eq. 8 makes the discrepancy between the theoretical and experimental plots for nanoelectrodes even stronger. Already this fact indicates that Eq. 8 and 9 do not apply to the case encountered in this study and suggest that the mechanism of Cu opd process on very small surfaces is at least slightly different from that observed at large Au(111) surfaces and gold microelectrodes (mechanism of Correia et al., see [23, 24]). Moreover, the electrode morphology, i.e. the presence of numerous defects on polycrystalline surfaces of micro- and nanoelectrodes, possibly influences the measured opd responses. The number of defects cannot be easily controlled; they might serve as additional crystallisation centres. For this reason, the current theories for metal deposition on very small electrodes still need some improvement and extension.

Acknowledgments Karolina Caban expresses her gratitude to Dr. Thomas Wandlowski for providing lab facilities and technical help, Dr. Gabor Meszaros for developing the experimental equipment and Dr. Dirk Mayer for fruitful discussions. The financial support of The Foundation for Polish Science is also gratefully acknowledged.

References

1. Grujicic D, Pesic B (2002) Electrochim Acta 47:2901
2. Barin C, Correia AN, Machado SAS, Avaca LA (2000) J Braz Chem Soc 11:175
3. Grubač Z, Metikoš-Huković M (2007) Mater Lett 61:794
4. Chen F, Qing Q, Ren L, Tong L, Wu Z, Liu Z (2007) Electrochim Acta 52:4210
5. Meszaros G, Kronholz S, Karthäuser S, Mayer D, Wandlowski T (2007) Appl Phys A 87:569
6. Li CZ, Tao NJ (1998) Appl Phys Lett 72:894
7. Li CZ, He HX, Tao NJ (2000) Appl Phys Lett 77:3995
8. Deshmukh MM, Prieto AL, Gu Q, Park H (2003) Nano Letters 3:1383
9. Xie FQ, Obermair Ch, Schimmel Th (2004) Solid State Comm 132:432
10. Xie FQ, Nittler L, Obermair Ch, Schimmel Th (2004) Phys Rev Lett 93:128303
11. Kervennic YV, van der Zant HSJ, Morpurgo AF, Gurevich L (2002) Appl Phys Lett 80:321
12. Morpurgo AF, Marcus CM, Robinson DB (1999) Appl Phys Lett 74:2084
13. Kashimura Y, Nakashima H, Furukawa K, Torimitsu K (2003) Thin Solid Films 438–439:317
14. Xiang J, Liu B, Wu ST, Ren B, Yang FZ, Mao BW, Chow YL, Tian ZQ (2005) Angew Chem Int Ed 44:1265

15. Qing Q, Chen F, Li P, Tang W, Wu Z, Liu Z (2005) Angew Chem Int Ed 44:1
16. Hölzle MH, Zwing V, Kolb DM (1995) Electrochim Acta 40:1237
17. Schneeweiss MA, Kolb DM (1999) Phys Stat Sol (a) 173:51
18. Scharifker B, Hills G (1983) Electrochim Acta 28:879
19. Hölzle MH, Apsel CW, Kolb DM (1995) J Electrochem Soc 142:3741
20. Gunawardena G, Hills G, Montenegro I, Scharifker B (1982) J Electroanal Chem 138:225
21. Abyaneh MY, Fleichmann M (1981) J Electroanal Chem 119:189
22. Abyaneh MY (1982) Electrochim Acta 27:1329
23. Correia AN, Machado SAS, Sampaio JCV, Avaca LA (1996) J Electroanal Chem 407:37
24. Correia AN, Machado SAS, Avaca LA (1994) J Braz Chem Soc 5:173
25. Aoki K, Osteryoung J (1981) J Electroanal Chem 122:19
26. Kolb DM (1996) Progress in Surface Science 51(2):103
27. Dakkouri AS, Kolb DM (1999) In: Wieckowski A (ed) Interfacial electrochemistry. Principles and applications. Dekker, NY
28. Dretschkow Th, Wandowski Th (2003) Topics Appl Phys 85:259
29. Leopold MC, Black JA, Bowden EF (2001) ACS Supporting Info
30. Woods R (1976) In: Bard AJ (ed) Electroanalytical chemistry vol 9. Dekker, NY
31. Marcus Y (1997) Ion properties. Dekker, NY
32. Heinze J (1993) Angew Chem Int Ed Engl 32:1268
33. Zhang XG, Li XH, Li HL (2001) J Coll Int Sci 243:68
34. Phanti KLN, Mohan S, Venkatachalam R (1991) Proc Indian Acad Sci (Chem Sci) 103:677
35. Quiroz MA, Morales U, Meas Y, Salgado L (1993) Rev Mex de Fisica 39:722
36. Hills G, Pour AK, Scharifker B (1983) Electrochim Acta 28:891
37. Shoup D, Szabo A (1982) J Electroanal Chem 140:237
38. Heerman L, Tarallo A (1998) J Electroanal Chem 451:101
39. Budevski E, Staikov G, Lorenz WJ (1996) Electrochemical phase formation and growth. VCH, Weinheim